FOKKER–PLANCK APPROACH OF OSTWALD RIPENING: SIMULATION OF A MODIFIED LIFSHITZ–SLYOZOV–WAGNER SYSTEM WITH A DIFFUSIVE CORRECTION*

THIERRY GOUDON† AND LAURENT MONASSE†

Abstract. We propose a well-balanced scheme for the modified Lifshitz–Slyozov equation, which incorporates a size-diffusion term. The method uses the Fokker–Planck structure of the equation. In turn, large time simulations can be performed with a reduced computational cost, since the time-step constraints are relaxed. The simulations bring out the critical mass threshold and the relaxation to equilibrium, which can be expected from the formal analogies with the Becker–Döring system.

1. Introduction. Ostwald ripening [40] is a physical mechanism that arises in many industrial, physical, or biological processes, like alloy formations [32, 33, 42], synthesis of quantum dots, emulsion dynamics (it is at the origin of the so-called "Ouzo effect" [44]), protein polymerization [23], etc. The mechanism can be described as an interaction between free particles, or monomers, and polymers, which can be seen as aggregates of monomers. Roughly speaking, the dynamics is governed by attachment to or detachment from polymers of monomers.

Having an accurate model for such phenomena is particularly important in material sciences. The models involve particle size distributions, describing the dynamics of mass exchanges between particles. A major advance is due to Lifshitz and Slyozov [33, 32] and Wagner [49], and their theory is widely considered as classical. An important prediction of the Lifshitz–Slyozov–Wagner (LSW) theory is the emergence of a universal profile, toward which all initial distributions evolve with time (up to an appropriate total-mass-rescaling). Such a conclusion is particularly relevant since the large time behavior usually corresponds to the observable states.

However, the conclusions of the LSW theory are subject to controversy. We refer the reader to [1, 4] for various aspects of the debate. The discussion is motivated by the combined improvements of the experiments [4] and of the numerical approaches [11, 10, 47]. Indeed, the LSW equations, which have the misleadingly simple form of a transport equation coupled to an integral constraint, present some hidden stiffness that makes the numerical problem singularly challenging: it is particularly difficult to capture the correct large time behavior, and one definitely needs dedicated schemes. Moreover, the mathematical analysis has also established the limitations of the LSW predictions [34, 36]. In particular, the large time behavior is highly sensitive to properties of the initial conditions.

There are several options to address these issues and to modify the original LSW model in order to clarify the asymptotic behavior of the solutions. The derivation of

the LSW equations assumes that the distance between clusters remains large so that
they do not interact directly; however, since the dynamics produces larger and larger
clusters, this assumption becomes questionable as time becomes large. Therefore,
the model can be completed by adding a coagulation term into the transport equa-
tion for macroscopic grains. This coagulation term is intended to restore a selection
mechanism of the LSW profile [33, section 3], an intuition that has been confirmed
on numerical grounds [47]. Another approach goes back to a discrete version of the
clusters population, where clusters are just seen as aggregates of a certain number of
monomers. One is led to an infinite set of ODEs, the Becker–Döring (BD) system
[5], which has a more standard asymptotic behavior than the LSW system: under a
certain critical mass condition, an equilibrium state can be identified, which indeed
attracts the solutions of the Cauchy problem [2, 3, 8, 6, 7, 25]. By rescaling appro-
priately the equations, the LSW system can be interpreted as the limit of the BD
equations [14, 41, 43]. Moreover, keeping a higher-order correction term in the equa-
tion, we obtain a modified LSW system, which involves a size-diffusion term. The
remarkable fact, pointed out in [21, 22], is that this correction restores formally the
equilibrium properties of the discrete model.

In this paper, we address the question of the numerical treatment of the modified
LSW system. We identify a structure which is common to that of the Fokker–Planck
equation and which makes the effect of relaxation to an equilibrium state appear.
Inspired by [26] for the (nonlinear) Fokker–Planck equation that arises in gas dynamics
and plasma physics, we design a numerical strategy of Finite Volume type which has
the Well-Balanced property: equilibria are automatically preserved, a crucial property
for large-time simulations. The scheme allows us to numerically check the conjecture
of the asymptotic trend to equilibrium.

The paper is organized as follows. In section 2 we review the basic facts about the
BD and LSW equations. In section 3, we detail the construction of the scheme, which
relies on a time-splitting and the resolution of a symmetric linear diffusion system.
We pay attention to discussing the stability issues that govern the choice of the time-
step. Section 4 is devoted to numerical experiments. In particular we compare the
scheme with a numerical approach recently designed in [27], based on an implicit-
explicit (ImEX) strategy, coupled with a high-order method for the discretization of
the transport term of the equation. Our findings can be summarized as follows:

- On the numerical side, the new scheme finds and preserves the expected equi-
  libria, it is less constrained by stability conditions and, therefore, it reaches
  large time simulations for a reduced numerical cost.
- On the modeling side, the simulation confirms the trend to equilibrium, with
  an exponential rate. These indications will be a motivation for further ana-
  lytical investigations, for instance inspired from the recent developments in
  [17].

2. From BD to LSW.

2.1. Discrete viewpoint: The BD system. We start by considering that
polymers are simply aggregates of i monomers, with i ranging over $\mathbb{N} \setminus \{0, 1\}$. Let
$t \mapsto c_i(t)$ stand for the concentration at time t of i-mers, and let $t \mapsto c_1(t)$ be the
monomers concentration. Mass-action kinetics apply to the reactions

$$(i) + (1) \rightleftharpoons (i+1),$$
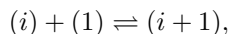
with coagulation rate a_i and fragmentation rate b_{i+1}, respectively. We are thus led to the BD equations [5]

$$(2.1) \qquad \frac{\mathrm{d}}{\mathrm{d}t}c_i = J_{i-1} - J_i \ \text{ for } i \geq 2,$$

with, for $i \geq 1$,

$$(2.2) \qquad J_i = a_i c_i c_1 - b_{i+1} c_{i+1}.$$

Monomers are involved in all of the reactions, thus the evolution of c_1 is driven by an equation with a different form

$$(2.3) \qquad \frac{\mathrm{d}}{\mathrm{d}t}c_1 = -2J_1 - \sum_{i=2}^{\infty} J_i.$$

At least formally, solutions of (2.1)–(2.3) satisfy

$$\frac{\mathrm{d}}{\mathrm{d}t}\sum_{i=1}^{\infty} i c_i(t) = 0,$$

which can be cast as a mass conservation property:

$$(2.4) \qquad c_1 + \sum_{i=2}^{\infty} i c_i = \rho \text{ is constant.}$$

Natural assumptions on the coefficients and the data can be summarized as follows:

$$a_i \leq Ci, \qquad b_i \leq Ci, \qquad \sum_{i=1}^{\infty} i^2 c_i(0) < \infty,$$

which allows us to establish the existence and uniqueness of globally defined solutions; see [3], and [31] for sharpened uniqueness results. Equilibrium solutions $(m_i)_{i\in\mathbb{N}\setminus\{0\}}$ of the BD system can be identified by imposing that the associated fluxes vanish: $J_i = 0$ leads to the recursion relation $m_{i+1} = \frac{a_i}{b_{i+1}}m_1 m_i$. (This defines the detailed balance equilibria, which are considered consistent with the microscopic reversibility principle from chemical kinetics.) Finally, we obtain a family of equilibrium states, parametrized only by the monomers concentration m_1

$$(2.5) \qquad m_i = Q_i m_1^i, \qquad Q_i = \frac{a_{i-1}a_{i-2},\ldots,a_1}{b_i b_{i-1},\ldots,b_2}.$$

We find the value of this parameter by going back to the mass constraint

$$(2.6) \qquad \sum_{i=1}^{\infty} i Q_i m_1^i = \rho.$$

This relation makes a threshold appear in connection with the notion of critical mass. Indeed, let μ_{crit} be the radius of convergence of the entire series in (2.6) (that is, when the limit exists, $\mu_{\mathrm{crit}} = \lim_{i\to\infty}\frac{b_{i+1}}{a_i}$) and set $\rho_{\mathrm{crit}} = \sum_{i=1}^{\infty} i Q_i \mu_{\mathrm{crit}}^i \in [0,\infty]$, the critical mass. The asymptotic behavior depends on whether or not the total mass ρ exceeds the critical mass ρ_{crit}: when $0 \leq \rho < \rho_{\mathrm{crit}}$, a monotonicity argument shows

that there exists a unique $m_1 \in (0, \mu_{\mathrm{crit}})$ such that $\sum_{i=1}^{\infty} i Q_i m_1^i = \rho$. This equilibrium is therefore a natural candidate for the asymptotic behavior of the solutions of the system with mass ρ, and the convergence to the equilibrium (in a strong sense) can indeed be justified [2, 3, 8], with rates that depend on the technical assumptions on the coefficients and the initial data [6, 7, 25]. When ρ exceeds the critical mass, as time becomes large the excess mass $\rho - \rho_{\mathrm{crit}}$ concentrates in larger and larger clusters, a phenomenon interpreted as a phase transition [3]. Technically, this phenomenon is reflected from the fact that $c_i(t)$ converges, as $t \to \infty$, weakly-$\star$ in the Banach space $\left\{ (u_n)_{n \in \mathbb{N}}, \ \sum_{n=0}^{\infty} n u_n < \infty \right\}$ to $m_{\mathrm{crit},i}$, the equilibrium state associated with the critical mass ρ_{crit}. For this supercritical situation the rate of convergence remains an open question.

2.2. Continuous viewpoint: The LSW system. In this description, which dates back to [32, 33, 42] and, independently, [49], roughly speaking, the polymers are assumed to have a "large" size compared to the monomers. However, they are not that large, so that direct interactions between clusters can still be neglected. The unknowns of the model are the size-density of polymers $(t, x) \mapsto f(t, x)$ and the monomers concentration $t \mapsto c(t)$. Given $\xi_2 > \xi_1 \geq 0$, the integral $\int_{\xi_1}^{\xi_2} f(t, x) \, \mathrm{d}x$ gives the number of polymers which have a volume $x \in (\xi_1, \xi_2)$. By the same token, the first order moment $\int_0^{\infty} x f(t, x) \, \mathrm{d}x$ defines the mass of the aggregates within the considered solution. The attachment and detachment processes are governed by principles of overall reduction of the interface energy, where volume effects, which favor growth, compete with surface effects, which favor dissolution. The description of these processes is embodied into two nonnegative coefficients a, b, that depend on the variable $x \geq 0$. The evolution is thus driven by

$$(2.7) \qquad \begin{aligned} &\partial_t f + \partial_x J = 0, \\ &J(t, x) = \big(a(x) c(t) - b(x) \big) f(t, x), \end{aligned}$$

coupled to the mass conservation constraint

$$(2.8) \qquad c(t) + \int_0^{\infty} x f(t, x) \, \mathrm{d}x = \rho \text{ is constant.}$$

A standard assumption requests

$$(2.9) \qquad a(0)\rho - b(0) \leq 0.$$

It means that the characteristics curves associated with the field $(t, x) \mapsto a(x)c(t) - b(x)$ are always pointing outward the domain $\{x \geq 0\}$, and, under this assumption, the equation does not need a boundary condition at $x = 0$. Moreover, the function $x \mapsto \frac{b(x)}{a(x)}$ is usually assumed to be nonincreasing so that at each time t a critical size $x_{\mathrm{crit}}(t) = \left(\frac{b}{a}\right)^{-1}(c(t))$ can be identified where the growth rate vanishes: it describes the fact that larger particles grow at the expense of smaller particles, which are thus assigned to become still smaller. We refer the reader to [13, 29, 30, 35, 37, 38] for the analysis of the existence-uniqueness issues for (2.7)–(2.8).

As pointed out in [41], adopting a suitable rescaling, the system (2.7)–(2.8) can be derived from the discrete model (2.1)–(2.3); see also the analysis in [14], and, more recently, in [43] where this question is revisited within the framework of the gradient flow structure of the equations. We equally refer the reader to [19] for a discussion on the case where (2.9) does not hold and how the connection with the discrete

modeling can help in finding a relevant boundary condition for (2.7)–(2.8) in this case, a situation which is relevant for applications in biology (assemblies of amyloid fibrils). Quite surprisingly, despite this natural connection with the BD system, the large time behavior of the solutions of (2.7)–(2.8) is completely different. Let us focus on the standard case where $a(x) = x^{1/3}$ and $b(x) = 1$. The asymptotic behavior can be summarized as

$$f(t,x) \underset{t \to \infty}{\sim} \frac{A_\rho}{(1+t)^2} \, M_K\Big(\frac{x}{1+t}\Big),$$

where $A_\rho = \rho\big(\int_0^\infty y M_K(y) \, \mathrm{d}y \big)^{-1}$ is a normalizing constant related to mass conservation, and $z \mapsto M_K(z)$ is a profile (which has an explicit expression), which depends on a certain constant $K \in \mathbb{R}$. Lifshitz and Slyozov [32, 33, 42] conjectured a selection process which defines a universal profile, associated with a specific value of the constant $K = K_{LS}$. However, both numerical simulations [10, 47] and mathematical analysis [34, 36] have shown that the selection of the profile is much more complicated: considering a data with compact support, the large time behavior selects K according to the shape of the initial data at the tip of the support! Such a phenomenon is highly unusual and it has motivated the introduction of sharp notions to describe the behavior of a function at the end of its support. Further details and references about the BD and Lifshitz–Slyozov systems can be found in the surveys [12, 24, 45].

2.3. A model with diffusive correction. The derivation of a continuous model from the discrete equations can be pushed forward: keeping the next terms in the asymptotic expansion leads to the following Fokker–Planck equation:

$$(2.10) \qquad \begin{cases} \dfrac{\partial}{\partial t}g + \dfrac{\partial}{\partial x}G(g;t,x) = 0, \\[2mm] G(g;t,x) = (a(x)c(t) - b(x))g - \varepsilon\dfrac{\partial}{\partial x}\left(\dfrac{a(x)c(t)+b(x)}{2}\,g(t,x)\right), \end{cases}$$

where $\varepsilon > 0$ is the scaling parameter. Equation (2.10) is supplemented by the mass conservation law

$$(2.11) \qquad c(t) + \int_0^\infty x g(t,x)\,\mathrm{d}x = \rho.$$

This model has been proposed in [21, 22] as a variant of the Lifshitz–Slyozov model. The asymptotic analysis further developed in [14] has also permitted us to identify a relevant boundary condition for (2.10); it reads

$$(2.12) \qquad \big(a(0)c(t) + b(0)\big)\, g(t,0) = \alpha\, c(t)^2.$$

The coefficient $\alpha > 0$ is reminiscient to the specific role of the aggregation between monomers to form 2-mers in the scaling adopted in [14]: the coupling between macroscopic clusters and (microscopic) monomers introduced by this reaction is considered to be weak; see also [18] for related observations.

Alternative versions of the diffusion corrections are discussed in [16, 17, 48]. In these papers the diffusion coefficients do not depend on the time variable, the properties of the coefficients a, b and the boundary condition are also different, which leads to completely different phenomena. We also refer the reader to [39] for a derivation of (much more intricate) diffusion corrections that goes back to an even more microscopic description by means of a mean-field regime.

Remark 1. It is worth explaining, at least formally, that the model (2.10)–(2.12) preserves the positivity of c, which is a crucial property in view of its physical interpretation. The argument is like that for the diffusionless Lifshitz–Slyozov equation; see [13]: we compute the time derivative of the first order moment

$$
\begin{aligned}
\frac{\mathrm{d}}{\mathrm{d}t} \int_0^\infty x g(t,x)\,\mathrm{d}x &= c(t) \int_0^\infty a(x) g(t,x)\,\mathrm{d}x - \int_0^\infty b(x) g(t,x)\,\mathrm{d}x \\
&\quad - \frac{\varepsilon}{2} \int_0^\infty \partial_x((a(x)c(t) + b(x))g(t,x))\,\mathrm{d}x \\
&= c(t) \int_0^\infty a(x) g(t,x)\,\mathrm{d}x - \int_0^\infty b(x) g(t,x)\,\mathrm{d}x + \frac{\varepsilon}{2}\alpha c^2(t)
\end{aligned}
$$

by taking into account (2.12). The constraint (2.11) implies that this is equally $-\frac{\mathrm{d}}{\mathrm{d}t}c(t)$. If c vanishes at time t_*, we get

$$
\frac{\mathrm{d}}{\mathrm{d}t}c(t_*) = \int_0^\infty b(x) g(t_*, x)\,\mathrm{d}x > 0.
$$

Then, either $t_* = 0$, and $c(t)$ becomes strictly positive for $t > 0$, or $t_* > 0$, with $c(t) > 0$ on $[0, t_*)$, which leads to a contradiction. Therefore, we have $c(t) > 0$ on $(0, \infty)$. (Note that this argument works with the homogeneous Dirichlet condition as in [16, 48], but it does not apply with the boundary condition proposed in [17].)

For the model (2.10), we obtain the following equilibrium solutions:

$$
(2.13) \qquad m_c(x) = m_c(0) \frac{a(0)c + b(0)}{a(x)c + b(x)} \exp\left(\frac{2}{\varepsilon} \int_0^x \frac{a(y)c - b(y)}{a(y)c + b(y)}\,\mathrm{d}y \right),
$$

where (2.12) gives

$$
m_c(0) = \frac{\alpha c^2}{a(0)c + b(0)}.
$$

This corresponds to the detailed balance equilibria that make the flux function G vanish. Therefore, we have a family of equilibrium states parametrized only by the monomers concentration c. The function $M : c \mapsto c + \int_0^\infty x m_c(x)\,\mathrm{d}x$ is well defined for $c \in [0, c_s)$, with $c_s = \limsup_{x \to \infty} \frac{b(x)}{a(x)}$; see [21, 22]. Let us denote $\rho_s = M(c_s)$. Observing that $c \mapsto M(c)$ is increasing, for any $\rho \in (0, \rho_s)$ we can find a unique $c \in (0, c_s)$ such that $M(c) = \rho$, which in turn defines uniquely the equilibrium with total mass ρ. We thus recover a similar discussion as for the BD system.

As a matter of fact, let us consider the simplest case where the coefficients a, b are constant. The equilibrium reads

$$
m_c(x) = \frac{\alpha c^2}{ac + b} \exp\left(\frac{2}{\varepsilon} \frac{ac - b}{ac + b} x \right).
$$

The critical mass is nontrivial when $0 < a < b$: $c_s = \frac{b}{a}$. Performing an expansion of the formulas for the equilibrium states of both the BD and (2.10) as c approaches the critical value, we are led to the following analogous formulae; see [21, 22]:

$$
m_i \simeq m_1 \exp\left(i \left(\frac{a m_1}{b} - 1 \right) \right), \quad m_c(x) \simeq c\,\frac{\alpha}{2a} \exp\left(\frac{x}{\varepsilon}\left(\frac{ac}{b} - 1 \right) \right).
$$

From this discussion, we can, therefore, expect that the diffusive model (2.10) restores the asymptotic properties of the BD system.

2.4. Further comments on different diffusive corrections. As mentioned in the previous section, other diffusive corrections to the Lifshitz–Slyozov equations have been proposed. However, they can describe different physical regimes, for which the present discussion is not relevant. In particular, the models discussed in [16, 17, 48] have the form

$$\partial_t g + \partial_x(Vf) = \partial^2_{xx}(Df)$$

with

$$V(t,x) = a(x)c(t) - b(x),$$

and the diffusion coefficient D *depends on the space variable only*. The parameter c is associated to a constraint that involves a moment of the unknown g:

- $c(t) = \frac{\int g\,dx}{\int x^{1/3} g\,dx}$, the inverse of the mean radius (which corresponds in the usual Lifshitz–Slyozov equation to prescribe $\int xf\,dx = \rho$; see, for instance, the derivation in [43]) [16], where the coefficients are given by $a(x) = x^{1/3}$, $b(x) = 1$, $D(x) = (1+x)^{1/3}$.
- $\int xg\,dx = \rho$, with the coefficients $a(x) = x^{1/3}$, $b(x) = 1$, $D(x) = x^{1/3}$ [48].
- $c(t) + \int_0^\infty A(x)g(t,x)\,dx$, with A a primitive of $x \mapsto \frac{a(x)}{D(x)}$ [17].

Note also that different boundary conditions are used to complete the problem: [16, 48] imposes the homogeneous Dirichlet condition $g(t,0) = 0$, while [17] uses $g(t,0) = \frac{1}{D(0)} e^{-B(0)+c(t)A(0)}$, with B a primitive of $x \mapsto \frac{b(x)}{D(x)}$. We can write the operator as

$$(2.14) \qquad L_c g = \partial_x\Big(DM_c\partial_x \frac{g}{M_c}\Big),$$

where

$$M_c(x) = \frac{D(0)}{D(x)} \exp\Big(\int_0^x \frac{a(y)c - b(y)}{D(y)}\,dy\Big).$$

In (2.14), this definition depends on the time variable through $c(t)$, as given from the constraint.

Note, however, that this formula for a given $c > 0$ does not define an admissible equilibrium solution for the equation proposed in [16, 48]: first, it is not compatible with the homogeneous Dirichlet condition; second, for the considered coefficients the first moment of M_c for any $c > 0$ is infinite. In other words, we have $c_s = 0$ in these cases. Therefore, the proposed approach is not designed for such situations. In particular, the analysis performed in [48] rather indicates that the asymptotic behavior is described, like for the original Lifshitz–Slyozov model, by means of a rescaled profile $g(t,x) \simeq \frac{1}{(1+t)^2}\Phi(\frac{x}{1+t})$, reflecting the formation of larger and larger clusters as time grows.

For the model in [17], one finds the equilibrium states

$$M_c(x) = \frac{A(x)}{D(x)} e^{A(x)c - B(x)}.$$

Again, with the coefficients considered in [17], $\lim_{x\to\infty} \frac{B(x)}{A(x)} = 0$ holds. However, the asymptotic analysis performed in [17] to establish convergence to equilibrium considers a noticeably different framework where c takes *nonpositive* values, and admissible equilibrium states are obtained for $c \le 0$. This describes a completely different physical regime where, contrarily to the standard Lifshitz–Slyozov model, the growth rate $V(t,x)$ is always nonpositive (which excludes to recover the features of the Lifshitz–Slyozov equation in the limit of small diffusion).

3. Numerical scheme. The numerical treatment of coagulation-fragmentation equations could be surprisingly challenging; many comments and further references for BD and LSW equations can be found, for instance, in [9, 10, 24, 47]. Here, we focus on the system with diffusion (2.10). In fact, the simulation of such a model is addressed in [27], using a coupling with a discrete model to describe interactions with the smallest clusters, instead of a boundary condition like (2.12). The numerical approach developed in [27] is based on a high order implicit Finite Volume method with slope limiters on advection. We point out that, in this approach, a proper high order accurate size discretization of the advection term turns out to be critical to obtain valuable results.

Here, we adopt a different viewpoint inspired from the numerical treatment of the Fokker–Planck equation in gas dynamics [26]. We split the resolution of the equation into two steps: the first step consists of solving the linear diffusion problem on g with c fixed, while the second step involves the numerical integration of the ODE in c.

3.1. Diffusion problem. With $c > 0$ given, let us consider the operator

$$L_c g = \partial_x \Big(-(ac - b)g + \frac{\varepsilon}{2}\partial_x(ac + b)g \Big).$$

Let us introduce the local equilibrium, parametrized by c,

$$M_c(x) = \frac{a(0)c + b(0)}{a(x)c + b(x)} \exp\Big(\frac{2}{\varepsilon} \int_0^x \frac{a(y)c - b(y)}{a(y)c + b(y)} \, \mathrm{d}y \Big),$$

which clearly makes the operator vanish: $L_c M_c = 0$. The use of M_c is equivalent to the use of m_c given by (2.13) but enables the treatment of extinction of monomers (see section 4.5). Then, the Fokker–Planck operator can be cast as

$$L_c g = \partial_x \Big(dM_c \partial_x \Big(\frac{g}{M_c} \Big) \Big)$$

with

$$d(x) = \frac{\varepsilon}{2} \Big(a(x)c + b(x) \Big).$$

Setting $h = \frac{g}{\sqrt{M_c}}$, it is convenient to define the operator

$$(3.1) \qquad \widetilde{L}_c h = \frac{1}{\sqrt{M_c}} L_c(h\sqrt{M_c}) = \frac{1}{\sqrt{M_c}} \partial_x \Big(dM_c \partial_x \Big(\frac{h}{\sqrt{M_c}} \Big) \Big),$$

which is symmetric for the usual L^2 inner product (in the sense that for all $\varphi \in C^\infty((0, +\infty), \mathbb{R})$ with compact support, $\langle \widetilde{L}_c h, \varphi \rangle_{L^2} = \langle h, \widetilde{L}_c \varphi \rangle_{L^2}$, similar to the Laplacian with nonhomogeneous Dirichlet boundary conditions). Such a change of unknowns which makes the operator symmetric already appeared for analyzing the BD system in [28]; see also [20]. Note that an alternative choice is $\overline{h} = \frac{g}{M_c}$, which yields the operator $\overline{L}_c \overline{h} = \frac{1}{M_c} \partial_x \big(dM_c \partial_x \overline{h} \big)$. In that case, the convergence to equilibrium of g is reflected by the convergence of $\overline{h}$ to a constant, which simplifies the interpretation of the outflow boundary conditions for large x. However, the operator $\overline{L}_c$ is not symmetric and the numerical resolution of the system is more involved in this case.

Given a mesh size Δx, the operator $\widetilde{L}_c$ is discretized by using the following for-

mula:

$$(3.2) \quad \frac{1}{\Delta x \sqrt{M_{c,j}}} \left(d_{j+1/2} \sqrt{M_{c,j+1} M_{c,j}} \frac{h_{j+1}/\sqrt{M_{c,j+1}} - h_j/\sqrt{M_{c,j}}}{\Delta x} \right.$$

$$\left. - d_{j-1/2} \sqrt{M_{c,j} M_{c,j-1}} \frac{h_j/\sqrt{M_{c,j}} - h_{j-1}/\sqrt{M_{c,j-1}}}{\Delta x} \right)$$

$$= \frac{1}{\Delta x^2} \left(d_{j+1/2} h_{j+1} - \frac{1}{\sqrt{M_{c,j}}} \left(d_{j+1/2} \sqrt{M_{c,j+1}} + d_{j-1/2} \sqrt{M_{c,j-1}} \right) h_j + d_{j-1/2} h_{j-1} \right).$$

Indeed, we wish to approximate (3.1) within the Finite Volume framework. On the cell $C_j = (x_{j-1/2}, x_{j+1/2})$, it is interpreted as $\frac{1}{\Delta x \sqrt{M_{c,j}}} (G_{j+1/2} - G_{j-1/2})$, where the numerical flux $G_{j+1/2}$ is intended to be an approximation of $dM_c \partial_x \left(\frac{g}{M_c} \right)$ on the interface $x_{j+1/2}$. To this end, the derivative is replaced by the centered finite difference $\frac{h_{j+1}/\sqrt{M_{c,j+1}} - h_j/\sqrt{M_{c,j}}}{\Delta x}$ and $M_c(x_{j+1/2})$ is approached by the geometric mean $\sqrt{M_{c,j+1} M_{c,j}}$. For further purposes, let us denote by S the corresponding matrix. Note that S is obviously symmetric in the case of Dirichlet boundary conditions, and Neumann boundary conditions only modify one diagonal coefficient which does not change the symmetry of S.

Having at hand a discrete distribution function g (which thus here is a vector with a size N given by the number of cells in the computational domain), we wish to update it by solving the linear problem

$$(3.3) \qquad g^{n+1} - \Delta t S g^{n+1} = g^n, \quad g_1^{n+1} = \frac{\alpha(c^n)^2}{a(0)c^n + b(0)}.$$

By using an implicit scheme we expect to relax the stability condition where Δt should be dominated by Δx^2, imposed by the diffusion operator. This is crucial when we wish to investigate the large time behavior of the equation. Note that the boundary condition on the right of the domain is left unspecified at the moment. In most numerical simulations, imposing a null flux ($G_{N+1/2} = 0$) is sufficient. Other choices are possible but lead to similar results, due to the exponential convergence of the size distribution to zero. However, in the supercritical mass case, the outflow of mass to ever larger cluster sizes requires adequate boundary conditions, as detailed in section 4.4.

Numerically, the computation of (3.2) can be difficult due to the fact that $M_c(x)$ displays extremely large or small values compared to $M_c(0) = 1$ for large x, with the exponential possibly exceeding the floating point capacities. In practice, we make use of the following expression for (3.2):

$$\frac{1}{\Delta x^2} \left(d_{j+1/2} h_{j+1} - \left(d_{j+1/2} \sqrt{\frac{M_{c,j+1}}{M_{c,j}}} + d_{j-1/2} \sqrt{\frac{M_{c,j-1}}{M_{c,j}}} \right) h_j + d_{j-1/2} h_{j-1} \right),$$

where the quotients of M_c are expressed as

$$\frac{M_{c,j+1}}{M_{c,j}} = \frac{a(x_j)c + b(x_j)}{a(x_{j+1})c + b(x_{j+1})} \exp \left(\frac{2}{\varepsilon} \int_{x_j}^{x_{j+1}} \frac{a(y)c - b(y)}{a(y)c + b(y)} \, dy \right).$$

In this expression the argument in the exponential remains of the order of $\mathscr{O}(\Delta x)$, while each of the $M_{c,j}$ could be very large. In addition, the expression only makes

use of local terms, in the sense that the integral is evaluated only on $[x_j, x_{j+1}]$ and does not depend on the rest of the domain. This is expected as a discretization of an elliptic differential operator and the property stems from the appropriate choice of $M_{c,j+1/2}$ as a geometric mean of $M_{c,j}$ and $M_{c,j+1}$.

3.2. Evolution of c. At the continuous level, expressing the conservation of total mass ρ, integration by parts leads to

$$\frac{\mathrm{d}}{\mathrm{d}t}c(t) = -\frac{\mathrm{d}}{\mathrm{d}t}\int_0^\infty xg(t,x)\,\mathrm{d}x = \int_0^\infty x\partial_x G(g;t,x)\,\mathrm{d}x$$

(3.4)
$$= -\int_0^\infty (a(x)c(t) - b(x))g(t,x)\,\mathrm{d}x - \frac{\varepsilon}{2}\alpha c(t)^2,$$

by using the boundary condition (2.12).

Applying a discrete analogue of the integrations by parts, assuming that g^n and g^{n+1} verify (3.3), the conservation of discrete mass $\rho^n = c^n + \sum_{i\geq 0} x_i g_i^n$ leads to

(3.5)　　$c^{n+1} - c^n = -\sum_{i\geq 0} x_i(g_i^{n+1} - g_i^n)\Delta x = \Delta t \sum_{i\geq 0} x_i(G_{i+1/2}^{n+1} - G_{i-1/2}^{n+1})$

(3.6)　　　　　　$= -\Delta t \sum_{i\geq 0} G_{i+1/2}^{n+1}\Delta x.$

Note that this is exactly the same expression as (3.4), except that the purely diffusive terms are not integrated here (the diffusive fluxes balance each other out, leaving only the boundary condition). Replacing with the expression of the numerical fluxes G, we find that defining

(3.7)　　　　$c^{n+1} = c^n + \Delta t \sum_{i\geq 0} d_{i+1/2} M_{i+1/2}\left(\frac{g_{i+1}^{n+1}}{M_{i+1}} - \frac{g_i^{n+1}}{M_i}\right)\Delta x$

exactly conserves total mass.

3.3. Splitting strategy. At time t^n, we have at hand a monomers concentration c^n and a vector $(g_1^n, \ldots, g_N^n)$ whose components are intended to be an approximation of $g(t^n, j\Delta x)$ for $j \in \{1, \ldots, N\}$. The right endpoint is chosen large enough so that a null flux boundary condition is correct (little to no flux to larger size clusters). When this hypothesis is invalid, alternative conditions can be imposed, as discussed in section 4.4. It allows us to construct

$$M_j^n = M_{c^n}(j\Delta x).$$

We set $h_j = \frac{g_j^n}{\sqrt{M_j^n}}$. Then, we obtain an intermediate quantity $h^\star$ by solving

(3.8)　　　　　　　　　$(\mathbb{I} - \Delta t S)h^\star = h + \beta,$

where $\beta = (\beta_1, \ldots, \beta_N)$ accounts for the boundary condition (2.12), namely all the components of β vanish but $\beta_1 = \Delta t d(0)\sqrt{\frac{\alpha|c^n|^2}{\Delta x^2(a(0)c^n + b(0))}}$. By construction the matrix S is symmetric and the linear system can be solved efficiently by the conjugate gradient algorithm. We set $g_j^{n+1} = h_j^\star\sqrt{M_j^n}$ and update the concentration c^{n+1} using (3.7).

Eventually it is worth pointing out that the scheme is, by construction, *well-balanced*: if the initial data is an equilibrium state, then the numerical solution remains at equilibrium forever.

3.4. Choice of the time-step. As noted previously, the implicit scheme on diffusion (3.3) is unconditionnally stable. The only stability criterion to be satisfied is the nonnegativity of the monomer concentration c, and we wonder whether the time-step is constrained by the preservation of this property. Suppose that the monomer concentration c^n at time t^n is nonnegative. Using (3.7) and (3.3), a sufficient condition for c^{n+1} to be nonnegative is

$$\Delta t |B^{\mathrm{T}}(\mathbb{I} - \Delta t L)^{-1}(g^n + \Delta t \bar{\beta})| \leq c^n,$$

where $L = M^{1/2} S M^{-1/2}$, $\bar{\beta} = \frac{\beta}{\Delta t}$, and B is the vector of general term

$$B_i = \begin{cases} - d_{1/2} \dfrac{M_{1/2}}{M_0} & \text{if } i = 0, \\[2mm] \dfrac{1}{M_i} \left(d_{i+1/2} M_{i+1/2} - d_{i-1/2} M_{i-1/2} \right) & \text{otherwise.} \end{cases}$$

Since the eigenvalues of L are nonpositive, a sufficient condition on Δt is

$$\Delta t |D^{-1}B||D(g^n + \Delta t \bar{\beta})| \leq c^n,$$

where D is any diagonal matrix. Using a triangle inequality, the scheme is stable as long as

$$(3.9) \qquad \Delta t \leq \frac{\sqrt{|Dg^n|^2 + 4\frac{c^n|D\bar{\beta}|}{|D^{-1}B|}} - |Dg^n|}{2|D\bar{\beta}|}.$$

In practice, a good choice for D is the diagonal matrix with d_i as diagonal elements. Note that with this choice, we observe in practice that the boundary condition contribution $\frac{c^n|D\bar{\beta}|}{|D^{-1}B||Dg^n|^2}$ is negligible, so that (3.9) reduces to the simpler expression in the absence of boundary conditions:

$$\Delta t \leq \frac{c^n}{|D^{-1}B||Dg^n|}.$$

Note that whereas condition (3.9) appears to be sharp for the fast initial phase of the system dynamics, it is suboptimal in the established regime: the variation of c becomes very slow and the term $|B^{\mathrm{T}}(\mathbb{I} + \Delta t L)^{-1}(g^n + \Delta t \bar{\beta})|$ tends to zero, while the norms $|D^{-1}B|$ and $|Dg^n|$ tend to a positive constant.

4. Numerical results.

4.1. Infinite critical concentration. Let us start with a few comments about the equilibrium states. In Figure 1 we plot the equilibrium functions for the coefficients

$$(4.1) \qquad a(x) = x^{1/2}, \qquad b(x) = 0.05 + 0.1 \times x^{2/3},$$

and several values of c. We have set $\alpha = 1.3$ and $\varepsilon = 0.05$. Note that in this case $c_s = +\infty$, $\rho_s = +\infty$ since fragmentation dominates for large clusters; the equilibrium functions are always admissible. We observe that the shape of the equilibrium is conserved. Note, in particular, that the function is not a simple bell shape, and there is a steep slope for small sizes. We observe that both the "support" (where the function takes significantly positive values) and the amplitude of the equilibrium varies a lot as a function of c (note that c varies in a quite tiny interval). This sensitivity can be a
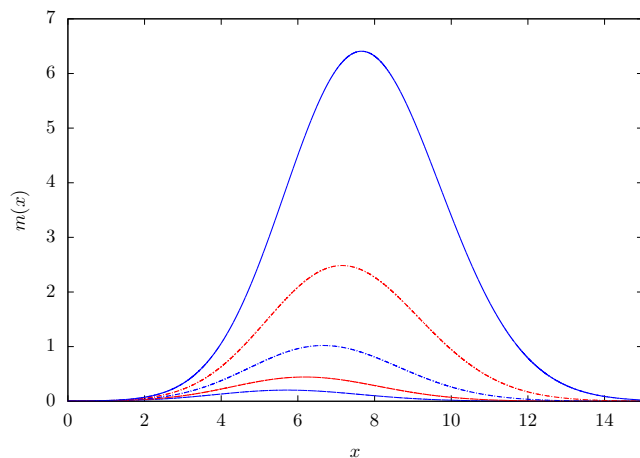
Fig. 1. *Equilibrium functions for the coefficients in* (4.1) *with c ranging over* $\{0.154, 0.155, 0.156, 0.157, 0.158\}$.
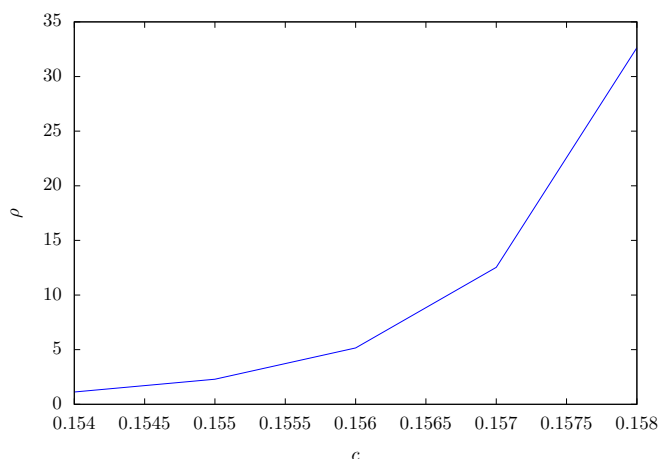

Fig. 2. *Total mass as a function of c for the coefficients in* (4.1).

numerical difficulty, since small errors on the monomers concentration can produce a large error on the equilibrium function. In Figure 2 we plot the variation of the total mass as a function of c for these equilibrium states.

In order to check the asymptotic behavior of the solutions of (2.10) we need to find a reference profile for the equilibrium function with a given total mass ρ. To this end, we simply use a dichotomy algorithm, exploiting the fact that $c \mapsto c + \int_0^\infty x m_c(x)\,dx$ is monotone. Figures 3–6 illustrate the evolution with the coefficients given by (4.1). The initial data reads

$$g(0, x) = 2e^{-40|x-0.5|^2}, \qquad c(0) = 1.6$$

so that $\rho = 1.8802$. The discretization step in size is fixed as $\Delta x = 1.5 \times 10^{-3}$ and the simulation domain is $[0, 15]$. The dichotomy procedure finds the equilibrium concentration $c_\infty = 0.1547$. In Figure 3 we plot the evolution of the monomers

concentration $t \mapsto c(t)$ and the total number of polymers $t \mapsto \int_0^\infty g(t, x)\, \mathrm{d}x$, up to the time $T = 10$. At first sight, one might believe that the equilibrium state is reached since $c(t)$ seems to go rapidly to the equilibrium value. However, the figure is a bit misleading: we have $c(T) = 0.1525$, and, going back to Figure 1, we realize that the corresponding local equilibrium is actually far from the expected final state. This metastability, due to the evolution of the stiffness of the problem, should not be mistaken with the asymptotic trend to equilibrium; see [9] for related comments about the BD equations. In fact the equilibrium profile requires considerably more time to establish: Figure 4 shows the polymers size distributions at several times, up to $T_f = 5000$. The successive cluster size distributions are represented in blue, with varying line style, while the equilibrium solution is represented in red. At $T_f = 5000$ the solution indeed becomes close to the equilibrium profile; see Figure 6, which shows how the solution, the local equilibrium, and the expected equilibrium coincide. The convergence of the monomers concentration c to the equilibrium concentration c_∞ and of the distribution of polymers g to the equilibrium profile m as $t \to +\infty$ is shown in Figures 7 and 8. The system appears to display an exponential convergence in time to the equilibrium. In contrast to the diffusionless Lifshitz–Slyozov equation, the behavior is similar when we start from a less regular initial state, say a step function, with the same mass. Figure 5 compares the solutions starting from a smooth initial distribution and a step function with the same mass. The cluster size distributions are represented in blue and red for the smooth initial distribution and the step function, respectively, with corresponding line styles at successive times. The solutions are clearly different for times less than 10, with the support of the step function remaining larger than that of the smooth initial distribution. Over long times, however, the solutions become indistinguishable and converge to the same equilibrium profile.
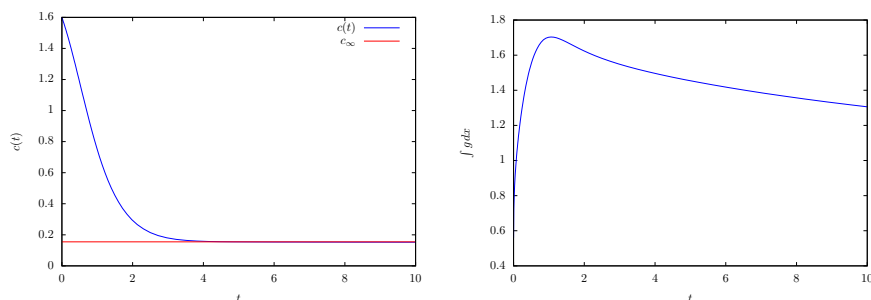

FIG. 3. *Evolution of $c(t)$ and $\int_0^\infty g(t, x)\, \mathrm{d}x$, up to the time $T = 10$, for the coefficients in* (4.1).

4.2. Comparison with an implicit-explicit scheme for advection diffusion. In order to assess the accuracy and efficiency of the present scheme, we compare the numerical results with an ImEx scheme for advection-diffusion. Equation (2.10) is discretized as follows:

$$(4.2) \qquad \frac{g^{n+1} - g^n}{\Delta t} + A_c g^n - D_c g^{n+1} = 0,$$

where A_c stands for the space-discrete advection operator with velocity $a(x)c - b(x)$ and D_c denotes the space-discrete diffusion operator associated to $\partial_x^2(d(x)\cdot)$. We opt for the natural centered discretization for D_c. The advection operator A_c is obtained with the MP5 scheme, which consists of a 5th order expansion with monotonicity
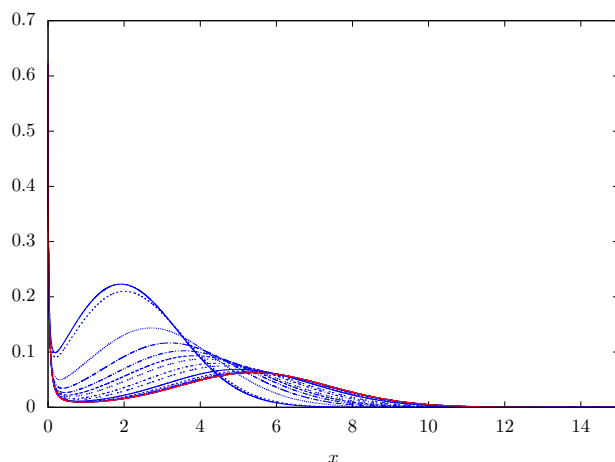
FIG. 4. *Polymer distribution function at several times for the coefficients in* (4.1) *up to the final time $T_f = 5000$.*
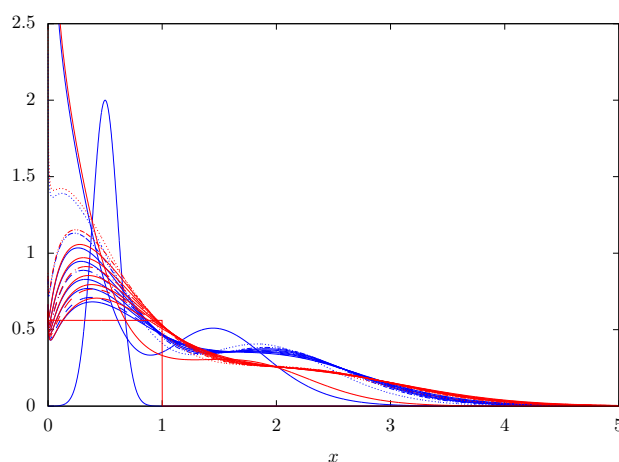

FIG. 5. *Polymer distribution function at times* $0, 1, 2, \ldots, 10$ *for the coefficients in* (4.1) *for initial Gaussian (blue) and step-function (red) distributions. (Figure in color online.)*

preserving flux limiting, as described in [27] (we also refer the reader to the original article of Suresh and Huynh for further reference [46]). The update of the monomer concentration is carried out in the same fashion as in section 3.2.

Figures 9 and 10 compare the convergence of the present scheme and the ImEx scheme to the asymptotic equilibrium state, for the monomer concentration and the size distribution, respectively. Note that the ImEx scheme error convergence saturates around $t = 8000$ due to the fact that it is not constructed to be well-balanced, contrary to the present scheme. This results in the ImEx scheme converge to a slightly inexact equilibrium state.

Regarding efficiency, the time-consuming tasks for each time-step consist of the linear solve (3.8) for the present scheme, and of the linear solve $(\mathbb{I} - \Delta t D_c)g^{n+1} = (\mathbb{I} - \Delta t A_c)g^n$ and the slope-limited advection $A_c g^n$ for the ImEx scheme. Since
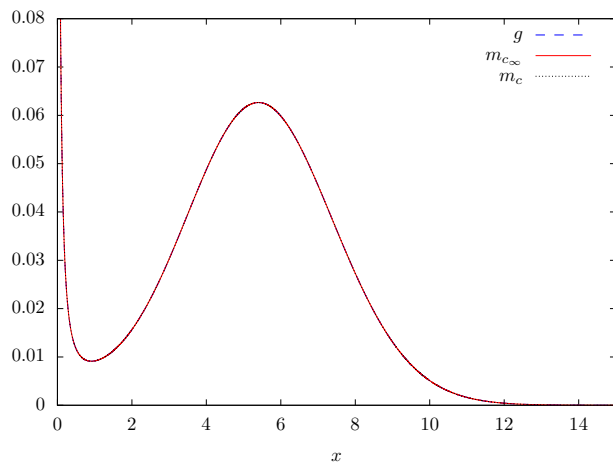
FIG. 6. *Polymer distribution function at the final time $T_f = 5000$, compared to the equilibrium profile, for the coefficients in* (4.1).
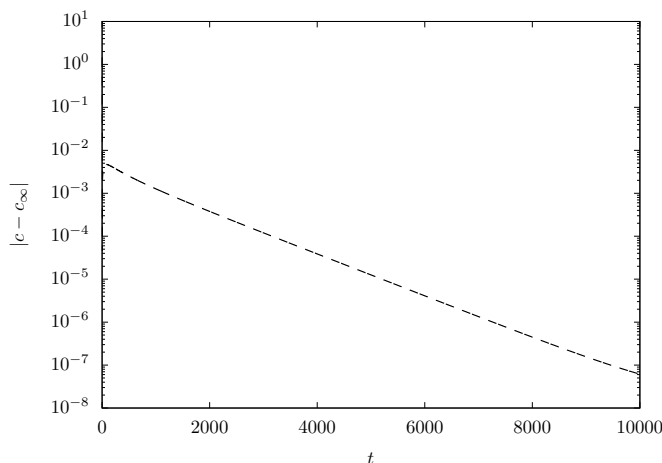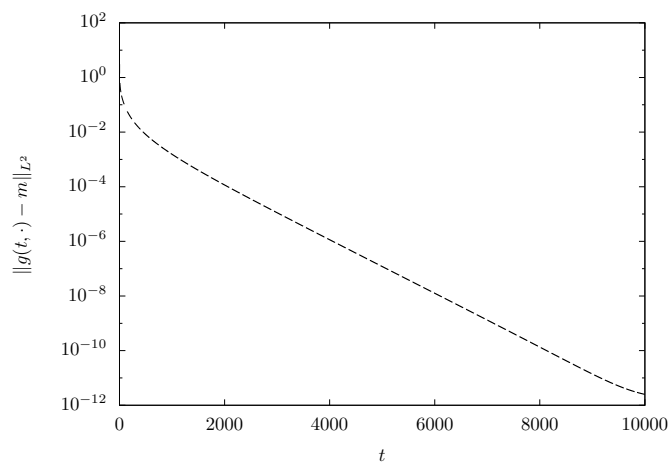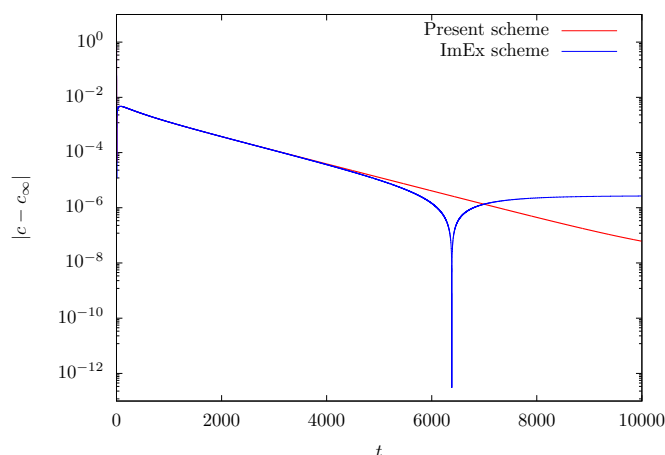

FIG. 7. *Evolution of $|c(t) - c_\infty|$ for the coefficients in* (4.1).

matrices $(\mathbb{I} - \Delta t D_c)$ and $(\mathbb{I} - \Delta t S)$ have similar conditioning, the cost for each time-step is comparable for both methods (with a slight advantage for the present scheme). It remains to compare the time-step stability condition on both schemes. The stability condition for the ImEx scheme is given by the classical Courant–Friedrichs–Lewy (CFL) condition on advection and the nonnegativity of the monomer concentration c (which depends only on the advection fluxes, since the diffusion fluxes cancel out):

$$(4.3) \qquad \Delta t \leq \min\left(\frac{\Delta x}{\max_{x \in [0,L]} a(x)c - b(x)}, \frac{c^n}{\Delta x \sum_{i=0}^{+\infty} F_i} \right),$$

where F_i denotes the advection flux which verifies $(A_c g^n)_i = \frac{1}{\Delta x}(F_{i+1} - F_i)$. We choose Δt as 10% of the maximal CFL conditions (3.9) and (4.3) for the present scheme and the ImEx scheme, respectively. The time-step evolution is compared in

FIG. 8. *Evolution of $\|g(t, \cdot) - m\|_{L^2}$ for the coefficients in* (4.1).

FIG. 9. *Evolution of $|c(t) - c_\infty|$ for the coefficients in* (4.1) *with the present scheme and the ImEx scheme.*

log-log scale for both schemes on Figure 11. We observe that in both cases, the time-step should be small in the initial part of the simulation, which can be related to the stiffness of the initial dynamics of the distribution. The time-step can then be increased around $t = 10$, which corresponds to c becoming close to the equilibrium value and the dynamics being dominated by the slow diffusion effects. Let us note that it is possible to take a time-step much larger, by one to two orders of magnitude, for the present scheme than for the ImEx scheme. The difference is particularly important for the long-term dynamics (after $t = 100$), which results in a significant difference in simulation time.

4.3. Finite critical concentration. We turn to a case where the critical concentration is finite. We set

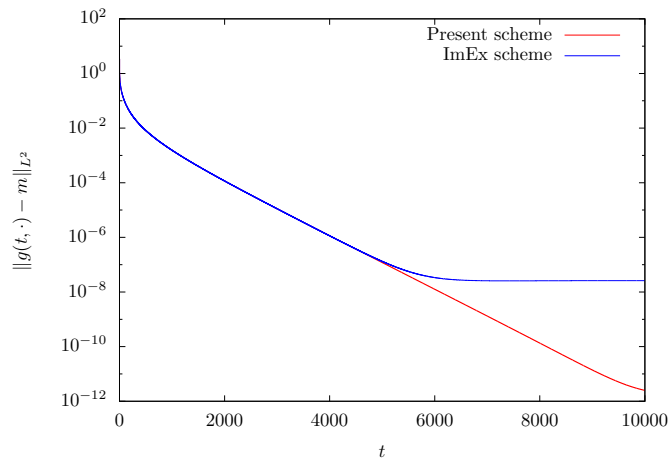(4.4) $$a(x) = 1 + x^{1/2}, \qquad b(x) = 0.1 + 0.75x^{1/2},$$

FIG. 10. *Evolution of $\|g(t, \cdot) - m\|_{L^2}$ for the coefficients in* (4.1) *with the present scheme and the ImEx scheme.*
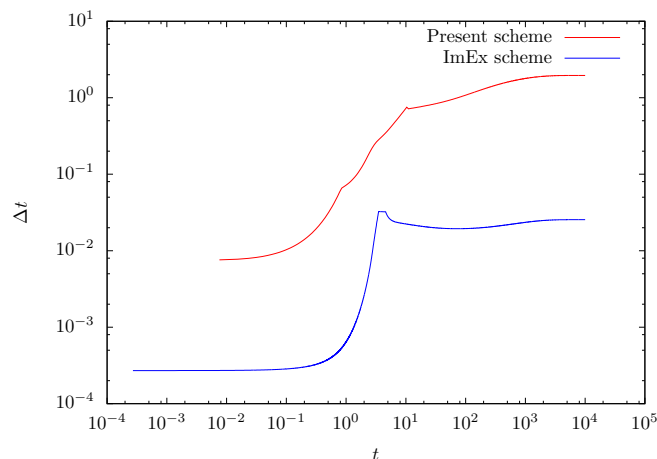

FIG. 11. *Evolution of the time-step in log-log scale for the coefficients in* (4.1) *for the present scheme and the ImEx scheme.*

with $\alpha = 0.001$ and $\varepsilon = 0.05$. We have $c_s = 0.75$ and $\rho_s = +\infty$ but difficulties appear clearly with smaller monomers concentration. Figure 12 shows the profiles that correspond to several values of c in the interval $[0.48, 0.51]$: we clearly observe the increase of the amplitude and the spreading of the support. Figure 13 illustrates how the total mass increases as a function of c.

We consider the evolution of the solution for the initial data

$$g(0, x) = 20 \ e^{-10|x-0.5|^2}, \qquad c(0) = 0.6.$$

The total mass for this initial condition is $\rho \approx 6.216$. The discretization step in size is $\Delta x = 1.5 \times 10^{-3}$ and the simulation domain is $[0, 30]$. Figure 14 shows the evolution of the monomer concentration which converges very slowly to the expected limit $c_\infty = 0.4987$; at the final time $T = 10000$, we find $c(T) = 0.4982$. The evolution of
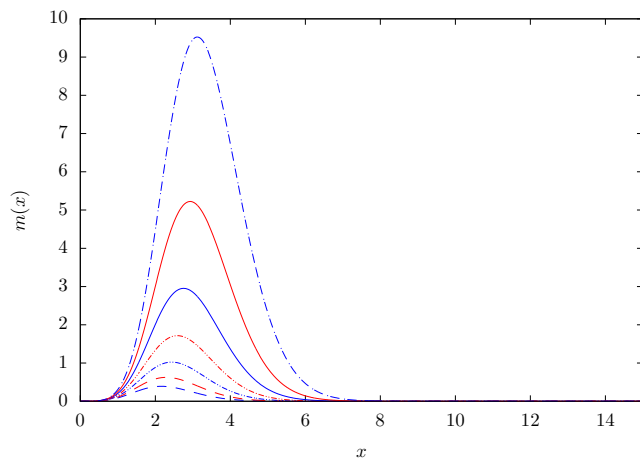
FIG. 12. *Equilibrium functions for the coefficients in* (4.4) *with c ranging over* {0.48, 0.485, 0.49, 0.495, 0.5, 0.505, 0.51}.
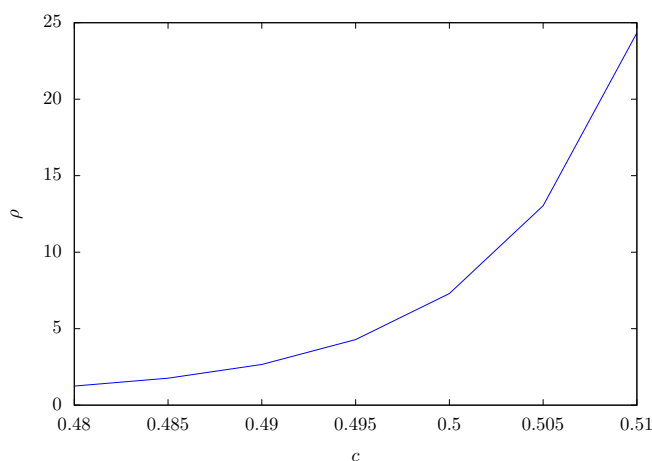

FIG. 13. *Total mass as a function of c for the coefficients in* (4.4).

the number of polymers is displayed in Figure 15. Accordingly, the asymptotic profile needs considerable time to establish. Figure 16 shows several polymer distributions up to the final time. The successive cluster size distributions are represented in blue, with varying line style, while the equilibrium solution is represented in red. Figure 17 compares the solution to the expected profile.

We now start with a different initial condition:

$$c(0) = 6, \qquad g(0, x) = \begin{cases} 0.4320194 & \text{if } x < 1, \\ 0 & \text{otherwise.} \end{cases}$$

Both initial conditions share the same (subcritical) mass, ensuring the existence of a steady state. However, the initial monomer concentration $c(0)$ is larger than the critical concentration $c_s = 0.75$. As a consequence, the present scheme involves operations with a diverging exponential function. However, as noted at the end of section 3.1, the
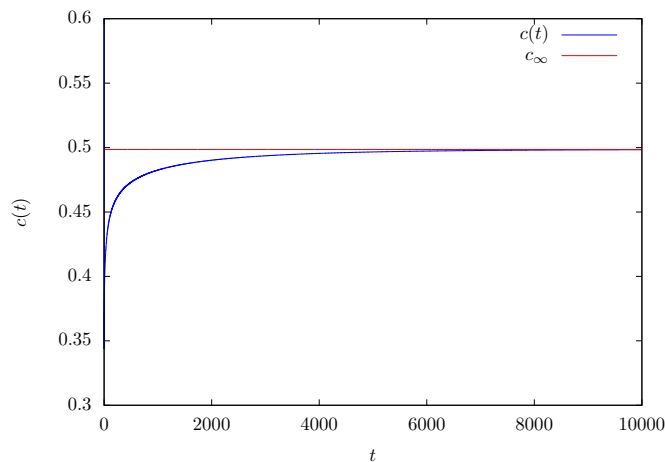
FIG. 14. *Evolution of $c(t)$, up to the time $T = 10000$, for the coefficients in* (4.4).
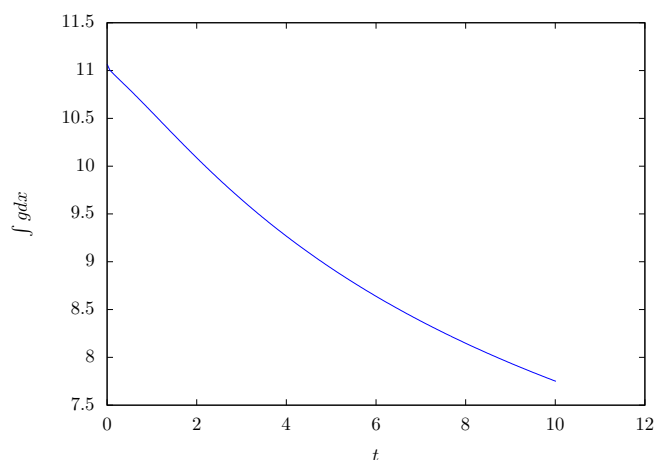
FIG. 15. *Evolution of $\int_0^\infty g(t,x)\, \mathrm{d}x$, up to the time $T = 10000$, for the coefficients in* (4.4).

formulation can be recast to eliminate the diverging exponential and nonlocal terms. In order to assess the robustness of the scheme in that case, we compare the present scheme with the ImEx scheme (which does not involve the diverging exponential). The comparison is carried out until $T = 10$, since Figure 18 shows that the monomer concentration $c(t)$ decreases under c_s as soon as $t > 2.03$. Figures 19 and 20 show the comparison of the solutions at times $t = 1$ and $t = 2$, respectively, for the present scheme and the ImEx scheme and for time-steps $\Delta t_1 = 4 \times 10^{-4}$ and $\Delta t_2 = 4 \times 10^{-5}$. We observe that while the two schemes differ with the larger time-step Δt_1 due to the added numerical diffusion, they are in close agreement for the fine time-step Δt_2. The use of a higher-order discretization of the elliptic operator L_c (we have tested order 4) does not improve significantly the results. Let us note that the time-step Δt_2 for which we observe convergence is small compared to the theoretical stability limits for the present and ImEx schemes: stability limit stands at the order of $\Delta t = 10^{-3}$
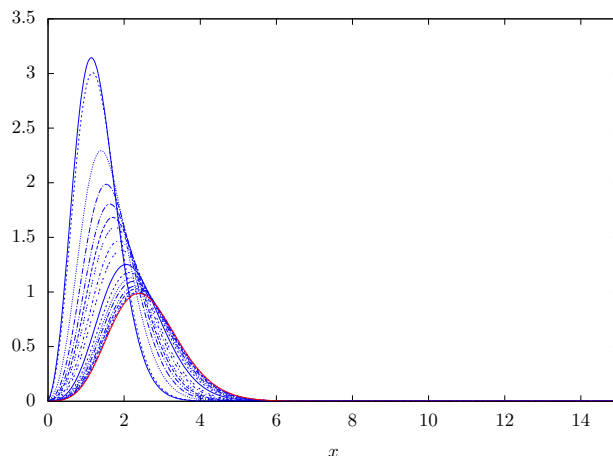
FIG. 16. *Polymer distribution function at several times for the coefficients in* (4.4) *up to the final time* $T_f = 10000$. *(Figure in color online.)*
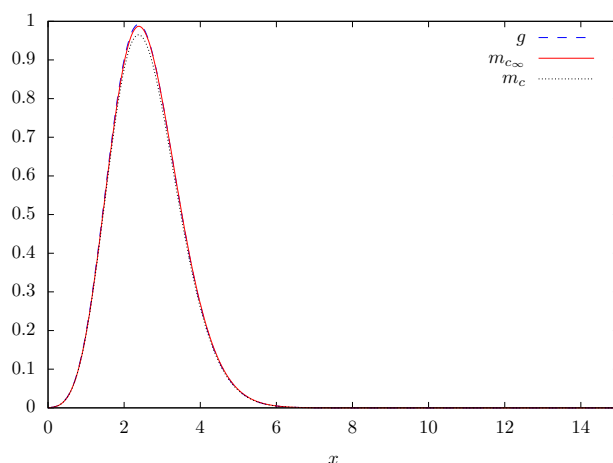

FIG. 17. *Polymer distribution function at the final time* $T_f = 10000$, *compared to the equilibrium profile, for the coefficients in* (4.4).

for the ImEx scheme and $\Delta t = 10^{-2}$ for the present scheme. Note, however, that the position of the peak size concentration is still adequately captured even for large time-steps and the present scheme is able to robustly accommodate the supercritical monomer concentrations until $c(t) < c_s$.

4.4. Finite critical mass and choice of the boundary condition on the right. We now study a finite critical mass case. We set

$$(4.5) \qquad a(x) = 1 + 5x^3, \quad b(x) = 1.5 + 5x^3,$$

with $\alpha = 100$ and $\varepsilon = 0.05$. We have $c_s = 1$ and $\rho_s \approx 1.655$. We consider the evolution of the solution for the initial data
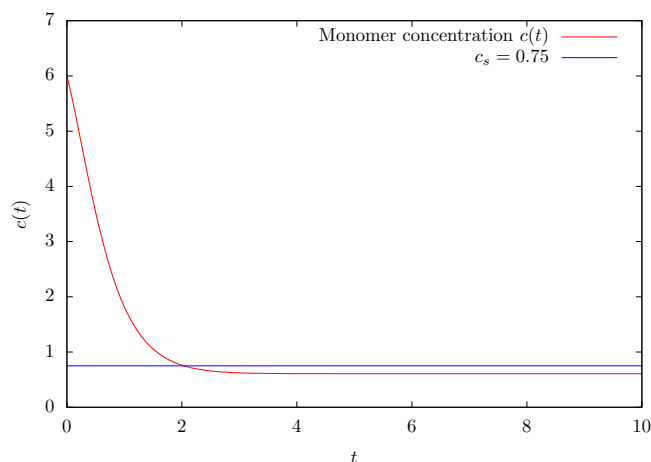
$$g(0, x) = \max(6(1-x), 0), \quad c(0) = 1.$$

FIG. 18. *Evolution of the monomer concentration $c(t)$ for the coefficients in (4.4) in the supercritical concentration case.*
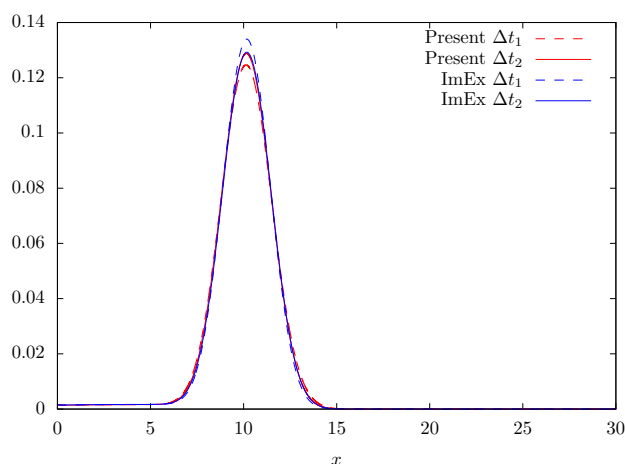

FIG. 19. *Solution at time $t = 1$ for the present scheme and the ImEx scheme for the coefficients in (4.4) in the supercritical concentration case, with time-steps $\Delta t_1 = 4 \times 10^{-4}$ and $\Delta t_2 = 4 \times 10^{-5}$.*

The initial condition satisfies $\rho = 2 > \rho_s$, which corresponds to the supercritical mass case. In this case, the mass excess $\rho - \rho_s$ should create ever larger cluster sizes, while the rest of the distribution (mainly contained inside the simulation domain) is expected to converge to the equilibrium state associated to ρ_s [3]. As a consequence, the choice of the boundary condition on the right is crucial since it conditions the mass flow from the simulation domain. In what follows, we denote by $[0, L]$ the simulation domain and by N the number of discretization points. In the numerical results, we take $L = 100$ and $N = 3 \times 10^4$.

We have studied four different boundary conditions. The first two conditions are straightforward: a homogeneous Dirichlet boundary condition ($g_{N+1} = 0$) and a null flux boundary condition ($G_{N+1/2} = 0$ or, equivalently, $\frac{g_{N+1}}{M_{N+1}} = \frac{g_N}{M_N}$). Note that the null flux is compatible with the existence with a nontrivial equilibrium state while the
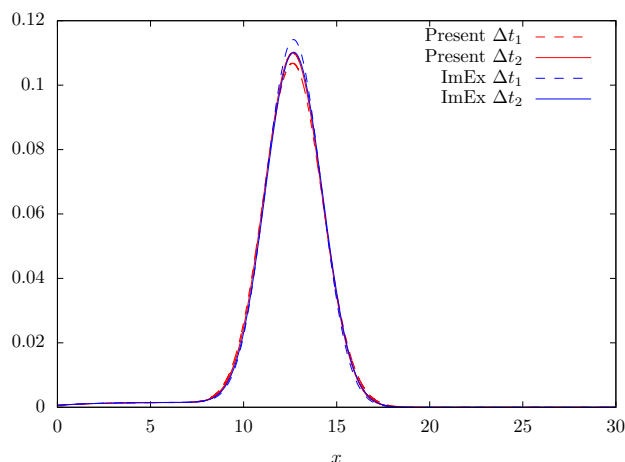
FIG. 20. *Solution at time $t = 2$ for the present scheme and the ImEx scheme for the coefficients in* (4.4) *in the supercritical concentration case, with time-steps $\Delta t_1 = 4 \times 10^{-4}$ and $\Delta t_2 = 4 \times 10^{-5}$.*
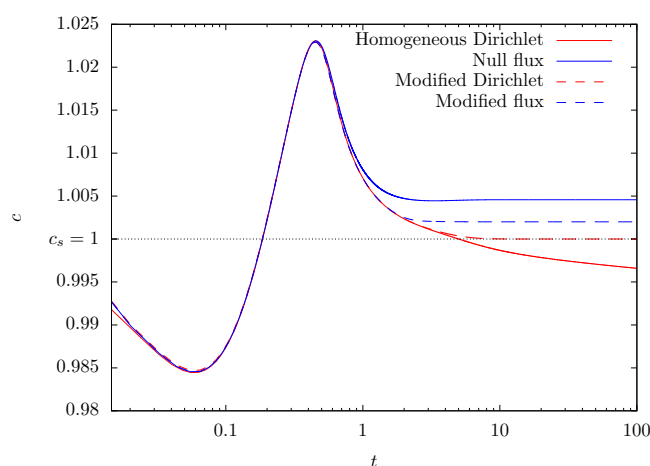

FIG. 21. *Evolution of the monomer concentration in the supercritical mass case for four different right boundary conditions: homogeneous Dirichlet, null flux, modified Dirichlet, and modified flux.*

homogeneous Dirichlet boundary condition is not, due to continued mass loss. On the other hand, the null flux condition is exactly mass-conservative and is unable to account for mass flowing to ever larger clusters outside the simulation domain. In order to mitigate these difficulties, we propose two alternative boundary conditions. First, a modified Dirichlet boundary condition consists of imposing the exact equilibrium state associated with the current monomer concentration c. However, when $c > c_s$, the diverging exponential induces extremely large values for g_{N+1}, which results in an explosion of the system. We therefore propose replacing c with $\tilde{c} = \min(c, c_s)$ and impose, in accordance with the left boundary condition (2.12),

$$g_{N+1} = \frac{\alpha \tilde{c}^2}{a(0)\tilde{c} + b(0)} M_{\tilde{c}}(x_{N+1}).$$

Similarly, the modified flux boundary condition writes

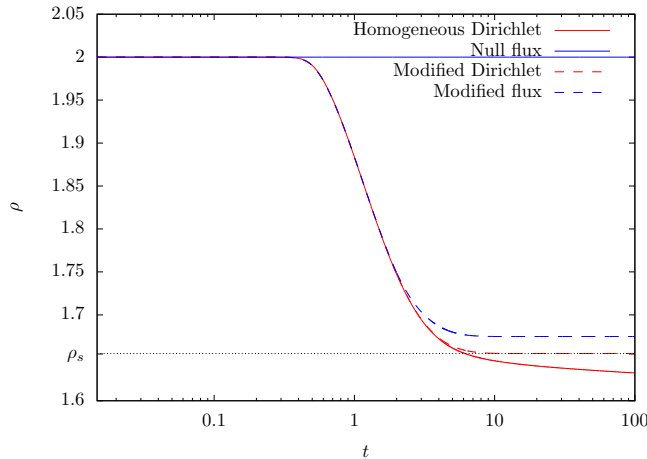$$\frac{g_{N+1}}{M_{\tilde{c}}(x_{N+1})} = \frac{g_N}{M_{\tilde{c}}(x_N)}.$$

FIG. 22. *Evolution of the total mass in the supercritical mass case for four different right boundary conditions: homogeneous Dirichlet, null flux, modified Dirichlet, and modified flux.*

The evolution of the monomer concentration c and of the total mass in the simulation domain ρ are shown in Figures 21 and 22, respectively, with a logarithmic scale in time to account for the change of system dynamics. We observe that, as expected, the null flux boundary condition enforces exact conservation of mass in the simulation domain and, consequently, the equilibrium monomer concentration c is larger than c_s. The homogeneous Dirichlet boundary condition loses too much mass, as predicted, and c does not converge to an equilibrium state (if continued, the simulation would show that c slowly tends to zero). On the contrary, the modified Dirichlet boundary condition and the modified flux condition display the correct general behavior: total mass in the simulation domain ρ decreases and reaches an equilibrium state, and the monomer concentration c converges to a constant. Quantitatively, we observe that the modified Dirichlet condition dissipates the correct amount of mass and converges to the theoretical exact solution with $c = c_s$ and $\rho = \rho_s$, while the modified flux condition does not dissipate enough mass.

The dynamics of the cluster size distribution is shown in Figure 23, with a logarithmic scale in size and distribution. We observe that for the first part of the dynamics ($t = 0.1$ and $t = 0.2$), the different boundary conditions are in good agreement, except for the modified Dirichlet boundary condition. This is due to the fact that the bulk of the cluster size distribution has not yet moved to the right and reached the right boundary of the domain, while the modified Dirichlet boundary condition imposes a boundary condition based on the monomer concentration c, resulting in an incorrect influx of information from the right boundary. However, from time $t = 0.4$, the different boundary conditions come into good agreement again: the limited pollution of the modified Dirichlet in the distribution tail has been smoothed by diffusion. Starting from $t = 1$, the different boundary conditions cause the solutions to diverge once again: the homogeneous Dirichlet boundary condition forces continued outflow from

the domain, while zero flux and modified flux conditions give inaccurate derivatives at the boundary of the numerical domain. Only the modified Dirichlet condition appears to give a correct distribution tail behavior.
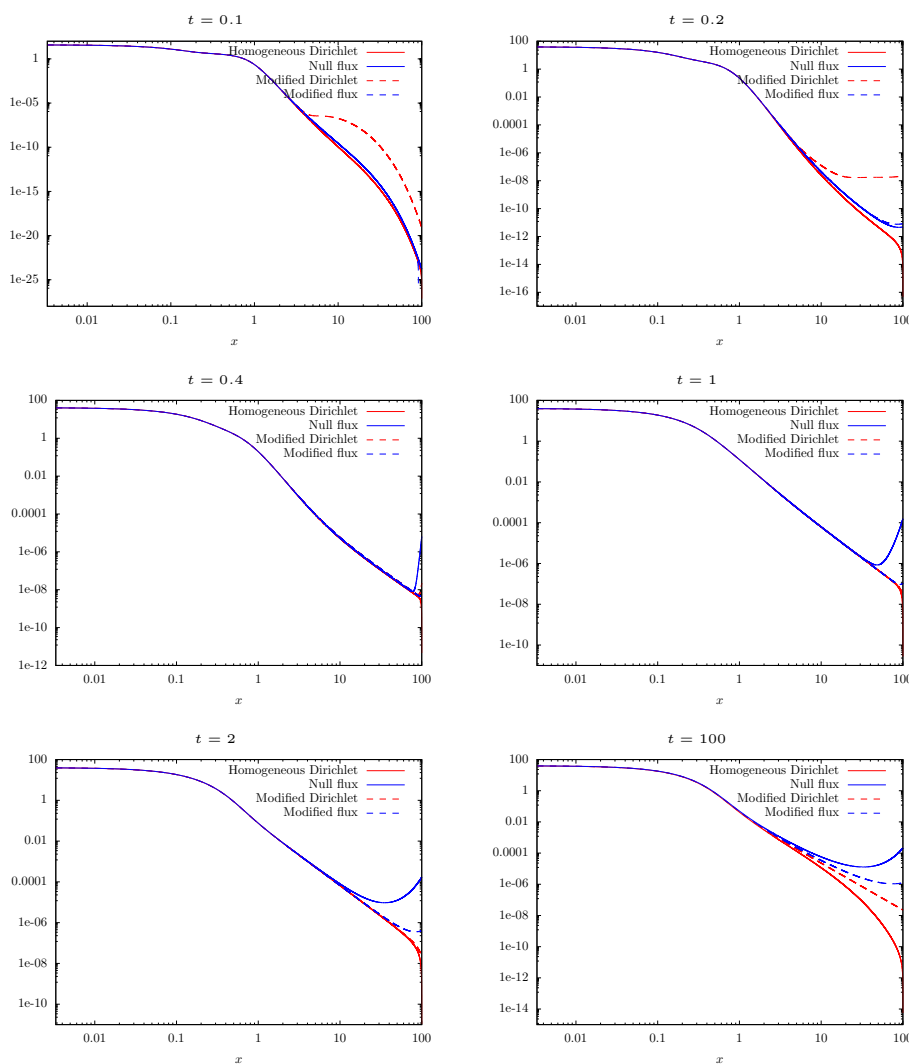

FIG. 23. *Solution at times $t = 0.1$, $t = 0.2$, $t = 0.4$, $t = 1$, $t = 2$, and $t = 100$ for the supercritical mass case for four different right boundary conditions: homogeneous Dirichlet, null flux, modified Dirichlet, and modified flux.*

4.5. Extinction of monomers. We now turn to the special case where there exists no nontrivial equilibrium state, due to the extinction of monomers. We set

$$(4.6) \qquad\qquad a(x) = 6 \times 10^5, \qquad b(x) = 0,$$

with $\alpha = 100$ and $\varepsilon = 1$. This case is similar to Case 4.1 in [27]. Since $b = 0$, no fragmentation occurs, so that the distribution shifts to ever larger clusters until the monomers are completely consumed.
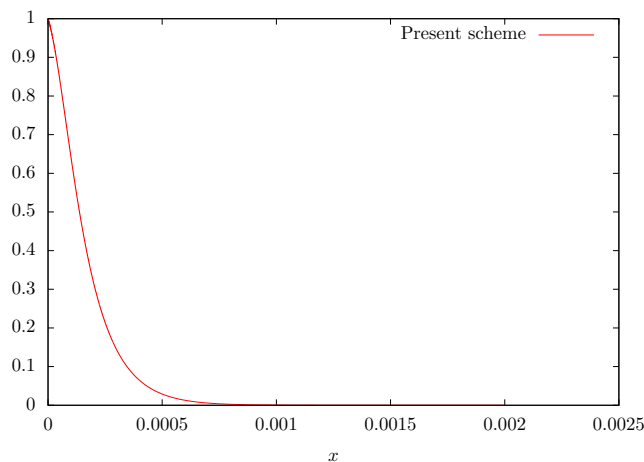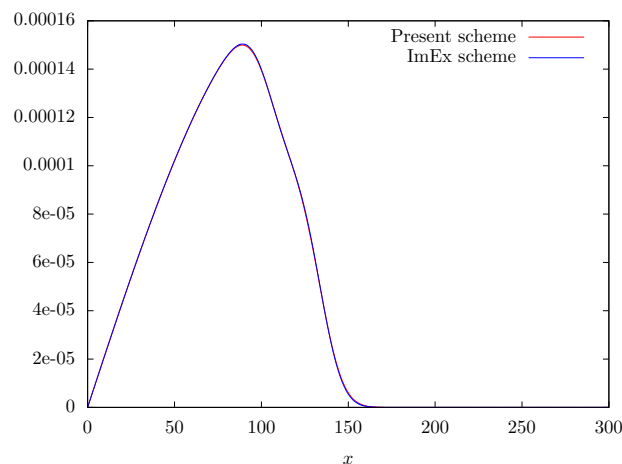
FIG. 24. *Monomer concentration evolution for case* (4.6).

FIG. 25. *Numerical solutions for case* (4.6) *at time* $t = 2 \times 10^{-3}$ *for the present scheme and the ImEx scheme.*

We consider the evolution of the solution for the initial data

$$c(0) = 1, \qquad g(0, x) = \begin{cases} 10^{-4} & \text{if } x < 30, \\ 0 & \text{otherwise.} \end{cases}$$

The discretization step in size is $\Delta x = 0.3$ and the simulation domain is $[0, 300]$. The concentration of monomers rapidly decreases to 0, as shown in Figure 24. The solution at final time $T = 2 \times 10^{-3}$ for the present scheme and the ImEx scheme is displayed in Figure 25. We observe an excellent agreement between the two schemes, using the same time-step for both schemes (set with the more restrictive ImEx CFL condition). This shows that the present scheme is capable of handling the simulation of supercritical cases, even when no equilibrium state exists.

5. Conclusion. We have proposed a well-balanced scheme for the LSW system with diffusion, which demonstrates its ability to capture accurately the long-time convergence to the equilibrium solution. The proposed scheme is more efficient than an ImEx scheme for advection diffusion on the test-cases studied. Even if designed originally for subcritical cases, the scheme is demonstrated to be capable of handling supercritical masses and even the extinction of monomers. However, the outflow boundary condition has to be handled adequately in order to recover the correct weak convergence to the critical equilibrium. The main drawback of the scheme is the inability to handle vanishing diffusion $\varepsilon = 0$. A future possible extension of the present work would be to investigate the (exponential in time) convergence to the equilibrium, based on discrete entropy arguments. We have checked that the entropy techniques developed in [15] do not apply directly here; the techniques presented in [17] for a very similar problem look quite appealing to handle this issue, but it would need nontrivial adaptations in order to deal with the different boundary conditions and properties of the coefficients.

REFERENCES

[1] A. BALDAN, *Review progress in Ostwald ripening theories and their applications to nickel-base superalloys part* I: *Ostwald ripening theories*, J. Materials Sc., 37 (2002), pp. 2171–2202.
[2] J. M. BALL AND J. CARR, *Asymptotic behaviour of solutions to the Becker-Döring equations for arbitrary initial data*, Proc. Roy. Soc. Edinburgh Sect. A, 108 (1988), pp. 109–116.
[3] J. M. BALL, J. CARR, AND O. PENROSE, *The Becker-Döring cluster equations: Basic properties and asymptotic behaviour of solutions*, Comm. Math. Phys., 104 (1986), pp. 657–692.
[4] P. L. BARRY AND T. PHILLIPS, *Trouble with Lifshitz, Slyozov and Wagner*, NASA Publications, 2003, https://www.nasa.gov/vision/earth/technologies/coarsening.html,
[5] R. BECKER AND W. DÖRING, *Kinetische Behandlung der Keimbildung in übersättigten Dämpfen*, Ann. Phys., 416 (1935), pp. 719–752.
[6] J. A. CAÑIZO, A. EINAV, AND B. LODS, *Trend to equilibrium for the Becker-Döring equations: An analogue of Cercignani's conjecture*, Anal. PDE, 10 (2017), pp. 1663–1708.
[7] J. A. CAÑIZO AND B. LODS, *Exponential convergence to equilibrium for subcritical solutions of the Becker-Döring equations*, J. Differential Equations, 255 (2013), pp. 905–950.
[8] J. CARR AND F. P. DA COSTA, *Asymptotic behavior of solutions to the coagulation-fragmentation equations. II. Weak fragmentation*, J. Statist. Phys., 77 (1994), pp. 89–123.
[9] J. CARR, D. B. DUNCAN, AND C. H. WALSHAW, *Numerical approximation of a metastable system*, IMA J. Numer. Anal., 15 (1995), pp. 505–521.
[10] J. A. CARRILLO AND T. GOUDON, *A numerical study on large-time asymptotics of the Lifschitz-Slyozov system*, J. Scient. Comp., 18 (2003), pp. 429–473.
[11] M. K. CHEN AND P. W. VOORHEES, *The dynamics of transient Ostwald ripening*, Modelling Simul. Mater. Sci. Eng., 1 (1993), pp. 591–612.
[12] J.-F. COLLET, *Some modelling issues in the theory of fragmentation-coagulation systems*, Comm. Math. Sci., 2 (2004), pp. 35–54.
[13] J.-F. COLLET AND T. GOUDON, *On solutions of the Lifschitz-Slyozov model*, Nonlinearity, 13 (2000), pp. 1239–1262.
[14] J.-F. COLLET, T. GOUDON, F. POUPAUD, AND A. VASSEUR, *The Becker–Döring system and its Lifschitz–Slyozov limit*, SIAM J. Appl. Math., 62 (2002), pp. 1488–1500, https://doi.org/10.1137/S0036139900378852.
[15] J.-F. COLLET, T. GOUDON, AND A. VASSEUR, *Some remarks on the large-time asymptotic of the Lifschitz-Slyozov equations*, J. Stat. Phys., 108 (2002), pp. 341–359.
[16] J. CONLON, *On a diffusive version of the Lifshitz-Slyozov-Wagner equation*, J. Nonlinear Sci., 20 (2010), pp. 463–521.
[17] J. G. CONLON AND A. SCHLICHTING, *A non-local problem for the Fokker-Planck equation related to the Becker-Döring model*, Discret. Contin. Dyn. Syst., 39 (2019), pp. 1821–1889.
[18] D. B. DADYBURJOR AND E. RUCKENSTEIN, *Kinetics of Ostwald ripening*, J. Crystal Growth, 40 (1977), pp. 279–290.
[19] J. DESCHAMPS, E. HINGANT, AND R. YVINEC, *Quasi steady state approximation of the small clusters in Becker-Döring equations leads to boundary conditions in the Lifshitz-Slyozov limit*, Comm. Math. Sci., 15 (2017), pp. 1353–1384.

[20] D. B. DUNCAN AND A. R. SOHEILI, *Approximating the Becker-Döring cluster equations*, Appl. Numer. Math., 37 (2001), pp. 1–29, https://doi.org/10.1016/S0168-9274(00)00020-9.

[21] S. HARIZ, *Une version modifiée du modele de Lifshitz-Slyozov: Existence et unicité de la solution, simulation numérique*, Ph.D. thesis, Université Nice Sophia Antipolis, Nice, France, 1999.

[22] S. HARIZ AND J.-F. COLLET, *A modified version of the Lifschitz-Slyozov model*, Appl. Math. Lett., 12 (1999), pp. 81–85.

[23] E. HINGANT, *Contributions à la modélisation mathématique et numérique de problèmes issus de la biologie: Applications aux prions et à la maladie d'Alzheimer*, Ph.D. thesis, Université Claude Bernard - Lyon I, Lyon, France, 2012.

[24] E. HINGANT AND R. YVINEC, *Deterministic and stochastic Becker-Döring equations: Past and recent mathematical developments*, in Stochastic Processes, Multiscale Modeling, and Numerical Methods for Computational Cellular Biology, D. Holcman, ed., Springer, Cham, 2017, pp. 175–204.

[25] P.-E. JABIN AND B. NIETHAMMER, *On the rate of convergence to equilibrium in the Becker-Döring equations*, J. Differential Equations, 191 (2003), pp. 518–543.

[26] S. JIN AND B. YAN, *A class of asymptotic preserving schemes for the Fokker–Planck–Landau equation*, J. Comput. Phys., 230 (2011), pp. 6420–6437.

[27] T. JOURDAN, G. STOLTZ, F. LEGOLL, AND L. MONASSE, *An accurate scheme to solve cluster dynamics equations using a Fokker-Planck approach*, Comput. Phys. Commun., 207 (2016), pp. 170–178.

[28] M. KREER, *Classical Becker-Döring cluster equations: Rigorous results on metastability and long-time behaviour*, Ann. Physik (8), 2 (1993), pp. 398–417, https://doi.org/10.1002/andp.19935050408.

[29] P. LAURENÇOT, *Weak solutions to the Lifschitz-Slyozov-Wagner equation*, Indiana Univ. Math. J., 50 (2001), pp. 1319–1346.

[30] P. LAURENÇOT, *The Lifschitz-Slyozov-Wagner equation with conserved total volume*, SIAM J. Math. Anal., 34 (2002), pp. 257–272, https://doi.org/10.1137/S0036141001387471.

[31] P. LAURENÇOT AND S. MISCHLER, *From the Becker-Döring to the Lifshitz-Slyozov-Wagner equations*, J. Statist. Phys., 106 (2002), pp. 957–991, https://doi.org/10.1023/A:1014081619064.

[32] I. M. LIFSHITZ AND L. PITAEVSKI, *Cinétique Physique*, Cours de Physique Théorique 10, L. Landau-I. Lifschitz, Mir, 1990.

[33] I. M. LIFSHITZ AND V. V. SLYOZOV, *The kinetics of precipitation from supersaturated solid solutions*, J. Phys. Chem. Solids, 19 (1961), pp. 35–50.

[34] B. NIETHAMMER AND R. PEGO, *Non-self-similar behavior in the LSW theory of Ostwald ripening*, J. Statist. Phys., 95 (1999), pp. 867–902.

[35] B. NIETHAMMER AND R. L. PEGO, *On the initial-value problem in the Lifschitz–Slyozov–Wagner theory of Ostwald ripening*, SIAM J. Math. Anal., 31 (2000), pp. 467–485, https://doi.org/10.1137/S0036141098338211.

[36] B. NIETHAMMER AND R. PEGO, *The LSW model for domain coarsening: Asymptotic behavior for conserved total mass*, J. Statist. Phys., 104 (2001), pp. 1113–1144.

[37] B. NIETHAMMER AND R. L. PEGO, *Well-posedness for measure transport in a family of nonlocal domain coarsening models*, Indiana Univ. Math. J., 54 (2005), pp. 499–530.

[38] B. NIETHAMMER AND J. J. L. VELAZQUEZ, *Global well-posedness for an inhomogeneous LSW model in unbounded domains*, Math. Ann., 328 (2004), pp. 481–501.

[39] B. NIETHAMMER AND J. J. L. VELAZQUEZ, *On screening induced fluctuations in Ostwald ripening*, J. Stat. Phys., 130 (2008), pp. 415–453.

[40] W. OSTWALD, *Studien über die Bildung und Umwandlung fester Körper*, Zeitschrift für physikalische Chemie, 22 (1897), pp. 289–330.

[41] O. PENROSE, *The Becker-Döring equations at large times and their connection with the LSW theory of coarsening*, J. Statist. Phys., 89 (1997), pp. 305–320.

[42] V. V. SAGALOVICH AND V. V. SLYOZOV, *Diffusive decomposition of solid solutions*, Sov. Phys. Usp., 30 (1987), pp. 23–44.

[43] A. SCHLICHTING, *Macroscopic limit of the Becker-Döring equation via gradient flows*, ESAIM:COCV, 25 (2019), 22, https://doi.org/10.1051/cocv/2018011.

[44] N. L. SITNIKOVA, R. SPRIK, AND G. WEGDAM, *Spontaneously formed transanethol/water/alcohol emulsions: Mechanism of formation and stability*, Langmuir, 21 (2005), pp. 7083–7089.

[45] M. SLEMROD, *The Becker-Döring equations*, Model. Simul. Sci. Eng. Technol., Birkhäuser Boston, Boston, 2000, pp. 149–171.

[46] A. SURESH AND H. T. HUYNH, *Accurate monotonicity-preserving schemes with Runge–Kutta*

time stepping, J. Comput. Phys., 136 (1997), pp. 83–99.

[47] L. M. TINÉ, T. GOUDON, AND F. LAGOUTIÈRE, *Simulations of the Lifshitz-Slyozov equations: The role of coagulation terms in the asymptotic behavior*, Math. Models Methods Appl. Sci., 23 (2013), pp. 1177–1215.

[48] J. J. L. VELÁZQUEZ, *The Becker-Döring equations and the Lifshitz-Slyozov theory of coarsening*, J. Statist. Phys., 92 (1998), pp. 195–236, https://doi.org/10.1023/A:1023099720145.

[49] C. WAGNER, *Theorie der Alterung von Niederschlägen durch Umlösen (Ostwald-Reifung)*, Zeitschrift für Elektrochemie, 65 (1961), pp. 581–591.